Journal of Sound and Vibration (1994) **173**(5), 683–698

PARTICLE REMOVAL BY FOCUSED ULTRASOUND

G. J. BRERETON AND B. A. BRUNO

Department of Mechanical Engineering and Applied Mechanics, University of Michigan, Ann Arbor, Michigan 48109, *U.S.A.*

(*Received* 14 *August* 1992, *and in final form* 22 *January* 1993)

An experimental study of the removal of micron particles from flat surfaces by focused ultrasonic waves has been carried out. The response of particles to acoustic forcing at gigahertz frequencies was studied by observation of manipulation and removal of individual particles, and by analytical and computational modeling of the mean acoustic removal forces. Consistencies between experiment and theory imply that secondary acoustic forces are of importance in contributing to a mechanism for removal, which is of the correct order to overcome surface-attractive forces on micron particles.

1. INTRODUCTION

In order to meet semiconductor industry goals of reduced line widths, it has become necessary to develop improved techniques for the removal of contaminants in the micron and submicron ranges. Existing cleaning methods such as wafer immersion in ultrasonic baths are unreliable when the contaminants are of the order of 1 μm, since the surface-attractive forces on particles of this size are so great. A promising alternative cleaning tool is the focused acoustic wave. When liquids are used to couple transducers to particle–surface systems, gigahertz excitation produces ultrasound at wavelengths commensurate in size with micron contaminants. Because ultrasound may be focused to beam widths as small as 1 μm, it offers opportunities for significantly higher acoustic power densities than undirected devices, together with spatial control over cleaning. The degree of localization also allows selective study of the response of individual particles to acoustic forcing, thereby facilitating characterization of particle removal by focused ultrasound.

There are several model problems which bear a relation to the removal of small particles from surfaces by acoustic forcing. The problem of a sphere in an infinite acoustic field has been treated by a number of researchers with differing levels of complexity. While the solution to the linear acoustic problem is well known (Morse [1]), analytical expressions for the plane-wave radiation pressure on rigid spheres in frictionless media have been deduced by King [2], and extended by Yosioka and Kawasima [3] to include compressible spheres. The corresponding results for spherical and cylindrical progressive waves [4, 5] are also available, while Danilov and Mironov [6] have extended some of these results to the case of wave propagation in viscous media, as have Temkin and Leung [7]. The model particle-removal problem of the interaction between a plane wave and a massless sphere attached to a surface by a stiff spring has recently been addressed using finite element potential-flow computations (Olson [8, 9]). The related problem of an elastic sphere attached by a spring and damper (to model Herzian contact and van der Waals attractive forces) to an elastic surface has been treated in a linear oscillator analysis by Geers and Hasheminejad [10]. Olson's computations revealed a monotonic increase in the size of

0022–460X/94/250683 + 16 $08.00/0

oscillatory forces with increasing acoustic frequency, whereas the analyses of Geers and Hasheminejad showed that the compliance at the surface/particle interface, the particle mass, and the added mass of fluid led to vibration resonance frequencies at wavelengths which were typically an order of magnitude longer than the particle diameter. The results of these linear problems may be used to estimate amplitudes of oscillatory forces acting on particles, whereas non-linear analyses are necessary to approximate any mean forces present.

There have been several experimental investigations in which selected particle–surface systems have been characterized according to the mechanical force necessary to overcome surface-attractive forces. Reed [11] has analyzed theoretical models for the adhesion of 10 μm diameter aluminum oxide particles to copper and steel substrates and compared his predictions with experimental results. Menon *et al.* [12] investigated the ultrasonic excitation levels necessary to effect removal of silicon, glass, and polystyrene latex (PSL) particles of prescribed size distributions from bare silicon and silicon dioxide wafers; they concluded that the levels required for removal were in proportion to the Hamaker constant of each material, in agreement with the London/Lifshitz model for van der Waals forces of attraction—the most important attractive forces between micron particles and a surface when immersed in a liquid. Menon *et al.* [12] also investigated particle detachment forces in terms of the surface tension forces which arise when a gas/liquid interface moves over the surface of a particle.

The effectiveness of ultrasonic cleaning processes has been investigated by Berg *et al.* [13] in a study in which several acoustic power parameters were varied in a systematic manner. Sound waves were typically radiated from a source at around 20 kHz, resulting in cavitation which caused both particle removal and surface damage (see Willard [14]). Their findings confirmed that large-scale cleaning effectiveness was proportional to the product of the average acoustic power and the exposure time. The macroscopic effectiveness of ultrasonic cleaning techniques has also been assessed by Kashkoush and Busnaina [15], who have made extensive measurements of particle removal efficiency as a function of particle diameter, ultrasonic duty cycle, frequency sweeps and other performance parameters. A more complete description of recent research into removal of particles from surfaces is given by Mittal [16, 17].

In summary, while a great deal is known about model problems with ideal geometries, this information has provided little understanding of the mechanics of particle removal. Macroscale experiments concerning many particles with irregular geometries and a distribution in sizes cannot be related simply to the results of a model acoustics problem. The approach described in this paper circumvents this difficulty by focusing a sound beam on individual particles and monitoring their response visually. The design of the focused ultrasound cleaner, its experimental performance, and comment relevant to mechanisms of removal of small particles from surfaces are described below.

2. DESIGN OF THE EXPERIMENT

An experiment for examining cleaning of micron particles with focused ultrasound was designed so that particles of known size could be introduced at a surface and their response to controlled ultrasonic excitation could be monitored. The experimental apparatus required for this study comprised electrical, acoustical, optical and mechanical subsystems which are described below.

2.1. ACOUSTIC DESIGN

An ultrasonic cleaner was designed around a Leitz acoustic microscope objective, rated for operation over the frequency range of 0·8–2·0 GHz. To maintain the attenuation at

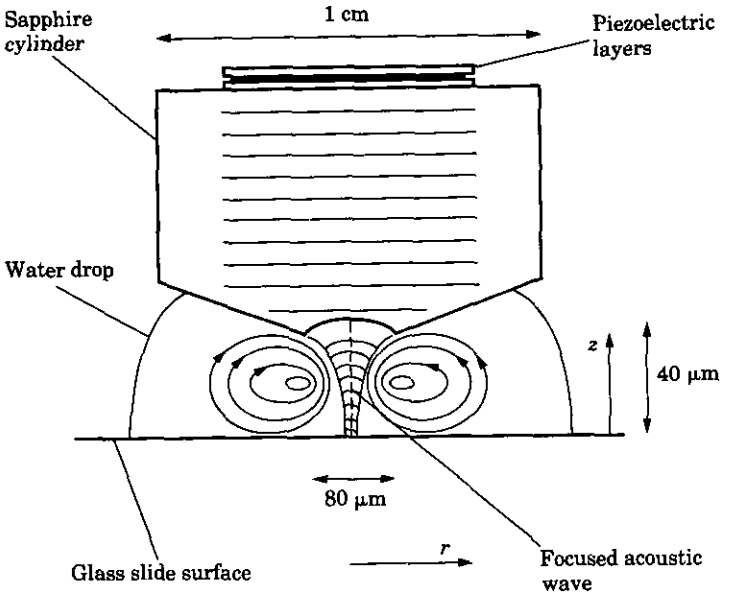

Figure 1. Acoustic transducer for focusing spherical waves in the gigahertz frequency range.

tolerable levels, the transducer was coupled to a contaminated surface with a water drop, as shown in the schematic drawing of Figure 1. The frequency range corresponded to wavelengths of approxiately 0·5–2 μm in water and so might be expected to maximize acoustic interaction with contaminants of that size. The short focal length of the objective (approximately 40 μm) ensured that the coupling liquid would remain in place through surface tension alone. It also kept the pathlength between the transducer and the surface well within the discontinuity distance at which weak shocks might occur, estimated at a few hundred wavelengths for gigahertz wave propagation at the expected power densities of a few W/cm^2. This estimate was based on approximate plane-wave solutions to the Navier–Stokes equations (see Beyer [18]) and was in general agreement with the finite element computation of Olson [8]. The short focal length and wavelength combined to yield a beam of narrow width at its focus which, when modelled as a focused disk of an initial diameter of 80 μm, had an Airy diameter (first zero of the Airy pattern) of 1·2 μm at 1 GHz.

The absorption coefficients for wave propagation at 1 GHz in water at 20°C typically take values as high as 220 cm^{-1} (assuming a quadratic dependence of absorption on frequency, as noted in Beyer [18]). Since this absorption is associated with dissipative losses, and it is the dissipation of acoustic energy flux that allows gradients in mean acoustic momentum flux to force acoustic streaming motions (see, for example, Lighthill [19]), streaming motions may be expected to accompany acoustic forcing.

2.2. ELECTRICAL DESIGN

The fragility of the piezoelectric layers at the upper transducer surface necessitated operation by pulse-width modulation to achieve acoustic power levels which were high enough to remove particles. Signal generators were therefore configured to control the transducer forcing frequency, the excitation period (typically several μs) and the duration between excitations (usually chosen as 10–20 μs) and so the duty cycle of the transducer; details of the circuitry are described by Schuck [20]. This mode of operation also allowed acoustic return signals to be monitored between periods of energization, by downmixing

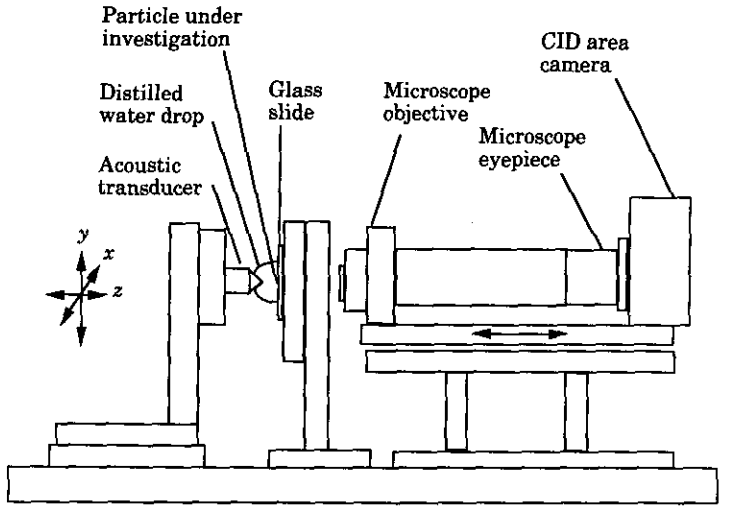

Figure 2. Optical and mechanical apparatus for ultrasonic interrogation and observation.

the reflected signal for display on an oscilloscope. This feature allowed the beam focus to be positioned on the slide surface by adjusting the z transverse (Figure 2) until the acoustic signal reflected from the surface was maximized. It also required the direction of ultrasound propagation to be normal to the surface, although oblique incidence could be investigated in a similar manner using two transducers of longer focal length.

The power delivered to the slide surface could be estimated by simple measurements and assumptions of attenuation reciprocity along the acoustic path. The incident power to the transducer was measured by replacing the transducer with a power meter and energizing the circuitry without gating. The reflected power was gauged from the oscilloscope voltage of the acoustic return signal, when the beam focus was at the slide surface. By assuming a loss of approximately 3 dB at the surface, and modelling the attenuation of water as 9 dB over 40 μm at 1 GHz ($\alpha \simeq 220\,\text{cm}^{-1}$, with energy attenuation over pathlength z modelled in the form $e^{-2\alpha z}$ [18]) the system attenuation characteristics were estimated as summarized in Table 1. During periods of energization, a typical level of power delivered to the transducer was 0·25 W, corresponding to about 0·35 mW delivered to the slide. If all power were focused within the Airy diameter of the beam, the local power density would be of the order of $10^4\,\text{W/cm}^2$. During these experiments, the greatest momentary power levels delivered to the transducer were of about 1 W.

2.3. OPTICAL AND MECHANICAL DESIGNS

The microscope system was designed using standard interchangeable objectives and an eyepiece, which allowed magnifications of 400×, 600× and 800×. The objective was

TABLE 1

System attenuation characteristics

Forward path through transducer	19 dB
Forward path through 40 μm of water	9 dB
Surface attenuation	3 dB
Return path through 40 μm of water	9 dB
Return path through transducer	19 dB
Total attenuation	59 dB

focused, through the back of a glass slide, onto the slide surface on which contaminant particles were present. The eyepiece was positioned to image onto a CID area camera, connected to a monitor and videocassette recorder. Lighting was provided in the form of a focused beam of incoherent light projected almost parallel to the slide surface, which allowed ample side-scattering of light from the particles at the slide surface to the microscope system. Resolution of particles of the order of a micron in diameter could then be achieved. The magnification powers of this optical arrangement (Figure 2) were calibrated using standard test gratings. The slide support was mounted on x–y–z traversing stages with micrometer controls for precise positioning of selected particles on the slide surface at the beam focus. The x and y stages could be interchanged with motorized ones for surface scanning operations.

3. EXPERIMENTAL PROCEDURES

Contaminated surfaces were prepared by spraying suspensions of particles (diamond, aluminum and PSL) onto the surfaces of microscope slides. The carrier fluid was a millimolar solution of a surfactant (Triton X-100) in distilled water, which acted as an anti-flocculent. After drying, the slide was mounted on its traversing stage and coupled to the acoustic transducer with a drop of distilled water. This technique allowed controlled contamination of surfaces with particles of known composition and size distribution, for subsequent acoustic interrogation. Provided that new slides (packaged under cleanroom conditions) were used, no significant differences in experimental results were observed when the contamination was carried out in either a cleanroom or under standard laboratory conditions.

Before examining the response of individual particles to acoustic excitation, the transducer was positioned so that the acoustic beam focus was at the slide surface. The position of the acoustic axis could then be determined visually, either by locating the axis of the streaming motions followed by a small number of particles injected into the water drop, or by identification of the axis relative to some feature of the transducer lens surface which was visible by microscope. The response of individual particles to controlled acoustic excitation could then be studied in a number of ways. For example, for a given duty cycle of excitation, the transducer could be positioned over a particle of interest and translated back and forth across the particle to see if any response could be observed: this procedure could then be repeated at small increments in frequency to search for resonant removal frequencies, postulated from linear theories applied to spherical particles. Other procedures used in this study included selecting particles and slowly increasing acoustic power until the particle was removed (while maintaining a fixed excitation frequency and duty cycle), or increasing the duty cycle to that necessary to remove particles at a fixed power level. All particle responses were recorded using standard video or high speed (Kodak Ektapro Motion Analyzer) video formats. The available response information was limited to particle presence/non-presence, displacement and removal trajectories, and streaming motion under conditions of controlled excitation.

4. EXPERIMENTAL RESULTS AND INTERPRETATION

The results reported in this section are experimental observations based on typical responses of 10–100 particles, and are not intended to provide reliable quantitative information. Factors such as inhomogeneous surface micro-characteristics and variation in the size and shape of individual particles are obviously important to the interpretation of individual observations and are essentially unmeasurable. Therefore, the aim of the

study was to deduce general trends and consistency between theory and results to the correct order of magnitude. These experimental observations and some physical interpretations are described in the following sections.

4.1. ACOUSTIC STREAMING AND PARTICLE REMOVAL

Experimental observation of the motion of particles injected into the water drop revealed recirculatory patterns, the centers of which formed a toroid around the acoustic axis (see Figure 1). The shape of these patterns and their apparently instantaneous acceleration and deceleration in response to changes in the applied power implied they were streaming motions driven by the focused beam. It has been speculated that these motions might remove particles by shear (Kashkoush and Busnaina [15]), although detailed experimental evidence is lacking. In this study, experimental observations were matched with computations of the streaming motions in the vicinity of the beam to estimate the streaming velocities and their shear force on particles.

The streaming motions which arise from the passage of a focused attenuated acoustic beam through a Newtonian liquid may be approximated through computations of the decomposed compressible Navier–Stokes equations. Following the method of successive approximations outlined by Rozenberg [21], in which pressure, density and velocity are decomposed according to their order (zero order—in the absence of the sound wave; first order—linear oscillatory variations in pressure, density and velocity owing to the sound wave propagation; second order—mean couplings of pressure, density and velocity of second order), one may approximate the governing equations at each order. Decomposing the dependent variables of pressure P, density ρ and velocity u_i as

$$P = P_0 + P_1 + P_2 + \cdots, \qquad \rho = \rho_0 + \rho_1 + \rho_2 + \cdots, \qquad u_i = u_{i_0} + u_{i_1} + u_{i_2} + \cdots,$$

the equations of continuity and linear momentum may be written at their various orders. While the equations of order zero merely confirm that ρ_0 is constant in the undisturbed fluid, the first order momentum equation takes the form:

$$\rho_0 \frac{\partial u_{i_1}}{\partial t} = -\frac{\partial P_1}{\partial x_i} + \frac{\partial}{\partial x_j}\left(\mu\left(\frac{\partial u_{i_1}}{\partial x_j} + \frac{\partial u_{j_1}}{\partial x_i}\right) + \delta_{ij}\lambda\frac{\partial u_{k_1}}{\partial x_k}\right), \tag{1}$$

from the linearity of which it is evident that an initially sinusoidal sound wave (of velocity u_{i_1}) remains sinusoidal and causes no change in the mean flow. In this equation, μ and λ are the first and second coefficients of viscosity, respectively. Of particular interest is the second order momentum equation, written as

$$\frac{\partial}{\partial t}(\rho_0 u_{i_2} + \rho_1 u_{i_1}) + \rho_0 u_{i_1}\frac{\partial u_{j_1}}{\partial x_j} + \rho_0 u_{j_1}\frac{\partial u_{i_1}}{\partial x_j} = -\frac{\partial P_2}{\partial x_i} + \frac{\partial}{\partial x_j}\left(\mu\left(\frac{\partial u_{i_2}}{\partial x_j} + \frac{\partial u_{j_2}}{\partial x_i}\right) + \delta_{ij}\lambda\frac{\partial u_{k_2}}{\partial x_k}\right). \tag{2}$$

Since an oscillatory acoustic velocity u_{i_1} implies an oscillatory first order variation in ρ_1 through continuity (see, for example, Beyer [18]), the time derivative of the product $\rho_1 u_{i_1}$ is also oscillatory. When equation (2) is averaged over time to describe the mean secondary motion, the entire time-dependent term makes no contribution, so that first order acoustic velocities contribute to the non-linear term on the left side as driving terms for the second order Stokes flow on the right side. A time-averaging operation also nullifies any average contribution of second order viscosity terms through the first order equation of continuity.

Given a reasonable description of the acoustic wave and boundary conditions in a suitable geometry, the second order equation may be solved by modifying standard elliptic Navier–Stokes programs such as derivatives of the TEACH code (Gosman *et al.* [22]). The

low Reynolds numbers of this problem renders this elliptic staggered-grid code quite adequate for such computations. For the geometries of this study, it was convenient to recast the second order streaming equations into an axisymmetric co-ordinate system in which the oscillatory first order equation of continuity, and the time-averaged second order equations of continuity, r-momentum and z-momentum took the form:

$$\frac{\partial \rho_1}{\partial t} + \frac{1}{r}\frac{\partial}{\partial r}(r\rho_0 v_{r_1}) + \frac{\partial}{\partial z}(\rho_0 u_{z_1}) = 0, \tag{3}$$

$$\frac{1}{r}\frac{\partial}{\partial r}(r\rho_0 \bar{v}_{r_2} + r\overline{\rho_1 v_{r_1}}) + \frac{\partial}{\partial z}(\rho_0 \bar{u}_{z_2} + \overline{\rho_1 u_{z_1}}) = 0, \tag{4}$$

$$\rho_0 \overline{v_{r_1}(\partial v_{r_1}/\partial r)} + \rho_0 \overline{u_{z_1}(\partial v_{r_1}/\partial x)} = -\frac{\partial \bar{P}_2}{\partial r} + \mu\left(\nabla^2 \bar{v}_{r_2} - \frac{\bar{v}_{r_2}}{r^2}\right), \tag{5}$$

$$\rho_0 \overline{v_{r_1}(\partial u_{z_1}/\partial r)} + \rho_0 \overline{u_{z_1}(\partial u_{z_1}/\partial x)} = -\frac{\partial \bar{P}_2}{\partial z} + \mu(\nabla^2 \bar{u}_{z_2}), \tag{6}$$

where the bar denotes a time-averaged quantity.

Exact solutions to the finite-amplitude wave equations are unavailable for spherical geometries in viscous media, so the approximate solution of Naugolnykh *et al.* [23] was used to model the acoustic velocity field in the form:

$$\frac{V}{V_0} = -\frac{r_0}{r}\,e^{-\alpha|r_0 - r|}\sin(\omega t - kr) + \frac{\lambda r_0}{2\pi r^2}\,e^{-\alpha|r_0 - r|}\cos(\omega t - kr)$$
$$+ e^{-2\alpha|r_0 - r|}\frac{r_0}{\lambda}\frac{V_0}{c}\pi\left(1 + \frac{B}{2A}\right)\frac{\ln(r/r_0)}{(r/r_0)}\sin 2(\omega t - kr). \tag{7}$$

This expression is approximately valid for propagation of a spherical waves beyond the immediate vicinity of the (diffraction affected) focus, where r is the local radius, V_0 is the initial particle velocity, r_0 is the initial radius, c is the acoustic velocity, α is the absorption coefficient at circular frequency ω, and B/A is a ratio of liquid thermodynamic properties [18]. The initial radius and particle velocity were evaluated as their values at the transducer surface and equation (7) was recast in axisymmetric form to describe v_{r_1} and u_{z_1} in equations (3), (4), (5) and (6). The focused acoustic wave was, therefore, modelled as a spherical wave over the appropriate solid angle.

Equations (3), (4), (5) and (6) were solved with the acoustic velocity field of equation (7) as the beam model, with V_0 estimated from the acoustic energy density at the lens/water interface using the transducer input power and the attenuations of Table 1. For the greatest power levels used in this study, this energy density $\langle E \rangle$ was approximately 2 kN/m^2. The initial particle velocity was estimated by taking $\langle E \rangle \simeq \rho_0 V_0^2/2$. The boundary conditions of three impenetrable rigid surfaces describing a regular cylindrical geometry were used with grids from 25 × 25 to 100 × 100. Different computational domains were used, ranging from dimensions as large as 1 cm to local domains resolved to the scale of a few microns. At distances of more than 1 mm from the beam, the flow was effectively at rest, and so the choice of a no-slip or a no-shear boundary condition at large radii was inconsequential to flow in the vicinity of the beam.

A sample computation for a power input of 200 mW ($\langle E \rangle \simeq 2$ kN/m^2 at the lens/water interface) at 1·0 GHz is shown in Figure 3(a), the near-surface region of which is shown in enlarged form in Figure 3(b). The toroidal streaming pattern may be seen clearly. The Reynolds number of the streaming flow ($U_{max} r_0/\nu$) was about 10^{-2} and so the assumption of Stokes flow was justified. The radial velocities were comparable to experimental measures (as the frame-to-frame displacement of suspended particles) which were of the

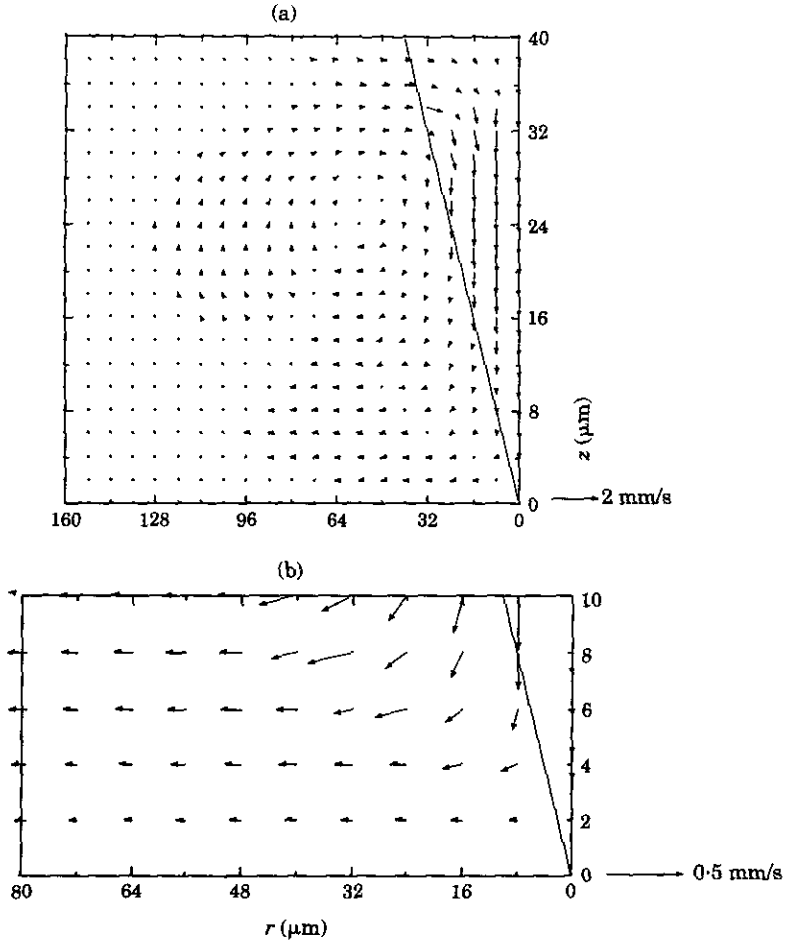

Figure 3. (a) Computation of the streaming velocity field in an axisymmetric cavity model of a water drop; the solid line marks the beam boundary within which the acoustic velocity is prescribed. $Re \simeq 0{\cdot}01$. (b) Near-surface region, close to the beam focus.

order of 0·1 mm/s in the region shown in Figure 3(b). The location of the axis of recirculation was within a few microns of that observed in experiments. Computations of larger domains, as shown in Figure 4, showed the same streaming motions. The insensitivity of these computations to the radial extent of the computational domain was

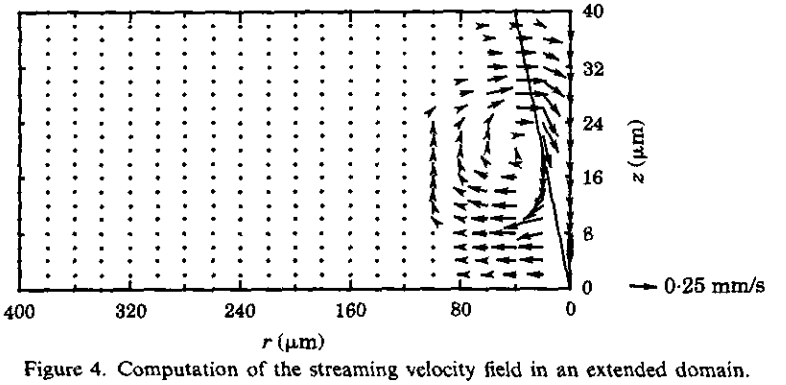

Figure 4. Computation of the streaming velocity field in an extended domain.

consistent with experimental observations that changes in water drop size had no noticeable effect on streaming.

The implicit assumption that at each order of approximation of P, u_i and ρ is much smaller than the preceding one may be expressed (Rozenberg [21]) as a constraint on the acoustic Reynolds number:

$$Re \ll \lambda L'/L''^2. \tag{8}$$

Here L' and L'' are the scale of the sound (first order) and streaming (second order) fields and Re is the acoustic Reynolds number. The confined geometry restricts L' and L'' to the same scale (~ 40 μm) and so for an acoustic Reynolds number $Re = \rho_0 V_0 \lambda/2\pi b$ (where b is the effective viscosity coefficient $2\rho_0 c_0^3 \alpha_0/\omega^2$ [21]) of 10^{-2} in this flow, this condition was satisfied easily.

From the computed streaming patterns of Figure 3(b), which were consistent with experimental observations, it is clear that within a few microns of the surface all velocities in the vicinity of the beam are of comparable order. Thus, viscous forces induced by radial streaming on all particles near the beam should be of similar size. By comparing the surface-attractive van der Waals force F_A with the applied drag force F_D (modelled as Stokes drag in a uniform stream) one may estimate the effectiveness of streaming as a means of particle removal under these conditions. The ratio of these forces takes the form:

$$\frac{F_D}{F_A} = \frac{3\pi\mu d U}{Bd/(3h^3)}. \tag{9}$$

The numerator is the Stokes drag on a sphere of diameter d, with slip velocity U, while the denominator models the van der Waals force, in which B is a particle–surface dependent coefficient. For particles used in these experiments, values of B were believed to be of the same order as those for silica particles in a vacuum, for which B takes the approximate value of 10^{-19} erg cm (Casimir and Polder [25]). This force ratio may be computed for various assumed distances of closest approach h of the particle to the surface. For $U \simeq 0{\cdot}1$ mm/s and $h/d \simeq 0{\cdot}01$ (a typical value used for smooth surfaces), this ratio is of order one for 10 μm particles. This result is consistent with experimental observation that large particles (5–15 μm) both adjacent to and as far as 60 μm from the beam focus could frequently be displaced along the surface during streaming at these velocities.

The linearity of Stokes flow, and the proportionality of acoustic energy density $\langle E \rangle$ to the advective acoustic velocity term on the left side of equation (2), implies that the streaming velocity increases in proportion to $\langle E \rangle$ and so to the power supplied to the transducer. This result was confirmed by experimental observations of Brereton and Bruno [24]. Therefore, for a constant value of h/d, equation (9) implies that Ud^3 (or $\langle E \rangle d^3$) must reach a given level for particle displacement by streaming to occur. However, the drag force imparted by streaming fluid has almost no surface-normal component according to the velocity vectors near the lower surface in Figures 3 and 4 and seems likely to cause rolling of particles along the surface. While these viscous forces might promote particle removal if a wafer were systematically swept with a focused cylindrical wave, the role of streaming in lifting particles from the surface appears to be negligible. The ratio of the lift force to the viscous drag force on a small sphere on a surface in a simple shear flow may be taken as $0{\cdot}287Re$ (Leighton and Acrivos [26], with Re as the hydrodynamic shear Reynolds number). For the characteristic Reynolds numbers of this study, lift forces generated by streaming on micron particles would be expected to be several orders of magnitude smaller than drag forces.

4.2. RADIATION PRESSURE, PARTICLE MANIPULATION AND PARTICLE REMOVAL

It was found that individual diamond particles (from 2 to 8 μm) could be manipulated about their points of contact with the surface through remote translation of the acoustic transducer at relatively low acoustic energy levels (i.e., $\langle E \rangle \simeq 2\,\mathrm{kN/m^2}$ at the lens/water interface for 1/20 of a 20 μs cycle). This effect is illustrated in Figures 5(a) and 5(b), in which photographs of a sequence of video frames are accompanied by a schematic of the phenomenon. The motion of the particle adjacent to the beam focus is a rotational one in which it realigns itself to present the most streamlined shape towards the axis of the acoustic beam. While drag forces exerted by streaming motions might account for this behavior, computations of the kind shown in Figure 3(b) indicate that there were comparable streaming velocities adjacent to more distant particles, which remained undisturbed. The localization therefore suggests an effect confined to the acoustic beam, such as an imbalance in radiation pressure forces around a particle as the transducer was moved.

When these experiments were carried out at higher acoustic energy densities ($\langle E \rangle \simeq 2\,\mathrm{kN/m^2}$ at the lens/water interface for 1/2 of a 20 μs cycle), the same particles were abruptly displaced along the surface, normal to the acoustic axis. Photographs of a sequence of video frames of removal events, together with a companion sketch of typical trajectories, are shown in Figures 6(a) and 6(b). It was also found that, for samples of particles of the same size and composition, removal was achieved when the *product* of acoustic energy and continuous exposure time reached an almost constant value (i.e., removal for either 1 μs pulses at $\dot{W} \simeq 500\,\mathrm{mW}$ or 2 μs pulses at $\dot{W} \simeq 250\,\mathrm{mW}$). This observation held for diamond particles, at a nominal 4 μm size, for pulses of duration of 1–20 μs and input power levels between 50 mW and 1 W. Approximately 20 particles were interrogated at each test condition.

While these observations are long-time averages of multiple short-time events, which cannot reveal details of removal mechanisms, they do indicate that particle removal does not depend solely on the applied power level or the amplitude of the acoustic wave. It is therefore interesting to consider the scale of secondary forces which might act in the vicinity of a focused acoustic beam, to see if they can effect removal. One such force is the radiation pressure force imparted by an unconfined, focused beam of ultrasound at an absorbing surface. While this force acts normal to a flat surface, in the direction in which the beam propagates, if the beam is directed against some part of a particle which rests on the surface, the interaction of focused ultrasound waves with that particle will impart a force on the particle which has some component in surface-parallel direction, as illustrated in Figure 7 and estimated below.

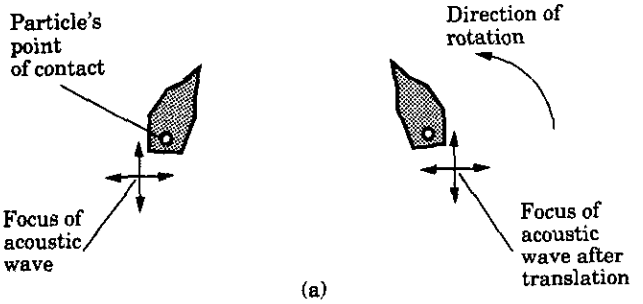

Figure 5. (a) Manipulation of a particle about its point of contact in a response to ultrasonic forcing. The left and right illustrations show particle orientation before and after transducer displacement. (b) A sequence of video images at 1/30 s intervals showing rotation of the upper 8 μm diamond particle, while the lower two are unaffected. The blurred spot is the left edge of the transducer, which is out of focus.

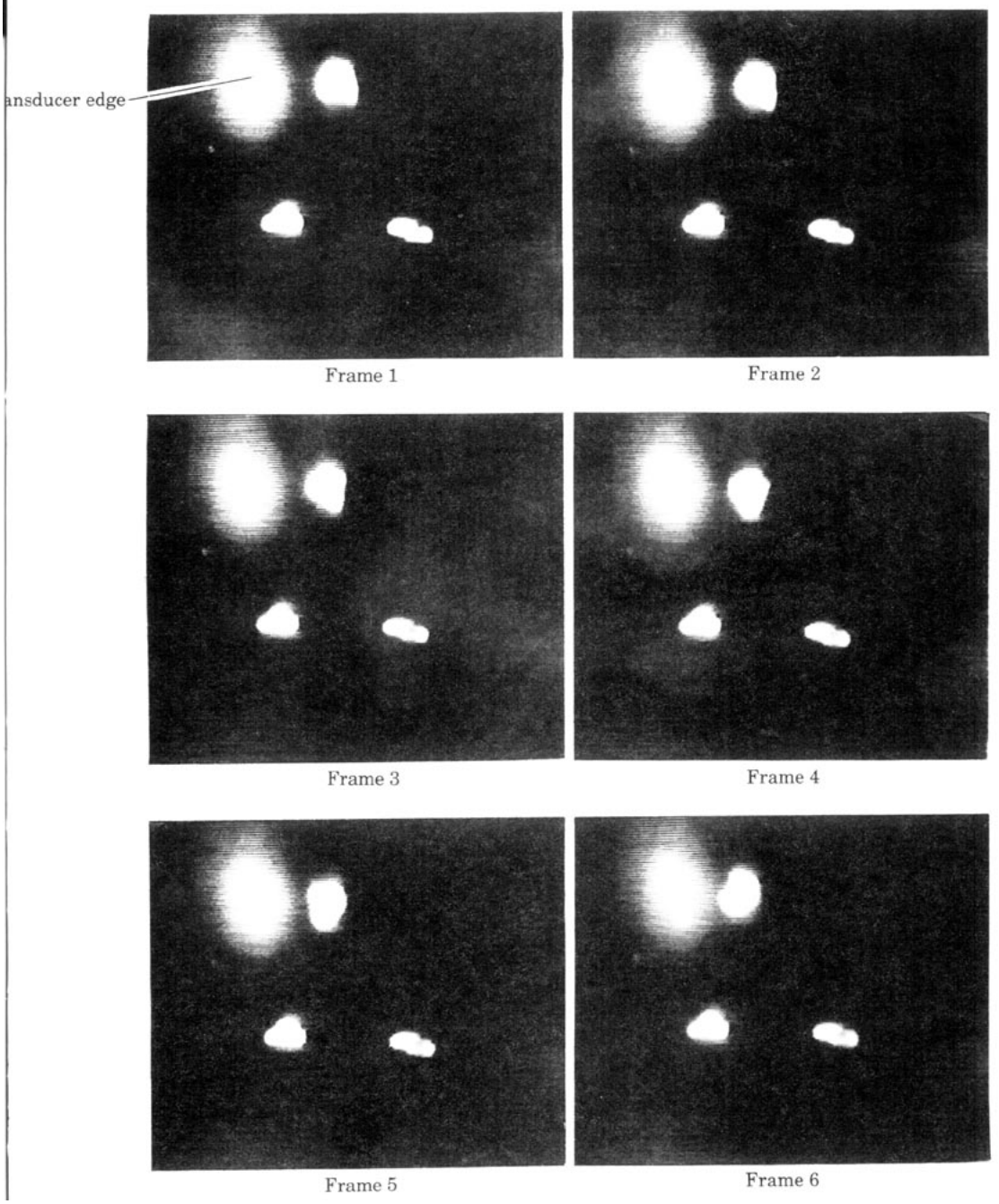

(b)

Figure 5—*continued.*

From Table 1, a typical transducer power input of 500 mW corresponded to delivery of 0·63 mW to a surface 40 μm from the transducer. The power input $\dot{W}$ may be related to the acoustic energy flux as

$$\dot{W} \simeq c(\pi D^2/4)\langle E\rangle, \tag{10}$$

so that, for a beam focused to a waist of $D \simeq 1$ μm, with $c = 1410$ m/s, $\langle E\rangle \simeq 390$ kN/m^2. The relevant radiation pressure experienced normal to a perfectly absorbing flat surface from an unconfined beam is the Langevin radiation pressure (Chu and Apfel [27]) represented by $\langle P_{rad}\rangle = \langle P^{Lgvn} - P_0\rangle = \langle E\rangle = 390$ kN/m^2. If it is assumed that the interaction of the sound wave with a particle on the surface imparts a force with some component normal to the particle surface of comparable order, then particles at the beam edge experience a net force in the outward radial direction. For the case of a micron particle positioned at the beam edge, the radiation pressure force represents the pressure difference acting on the particle cross-sectional area. The ratio of this force to the surface attractive one may then be estimated as

$$\frac{F_{rad}}{F_A} = \frac{\langle P_{rad}\rangle \pi d^2/4}{Bd/(3h^3)}, \tag{11}$$

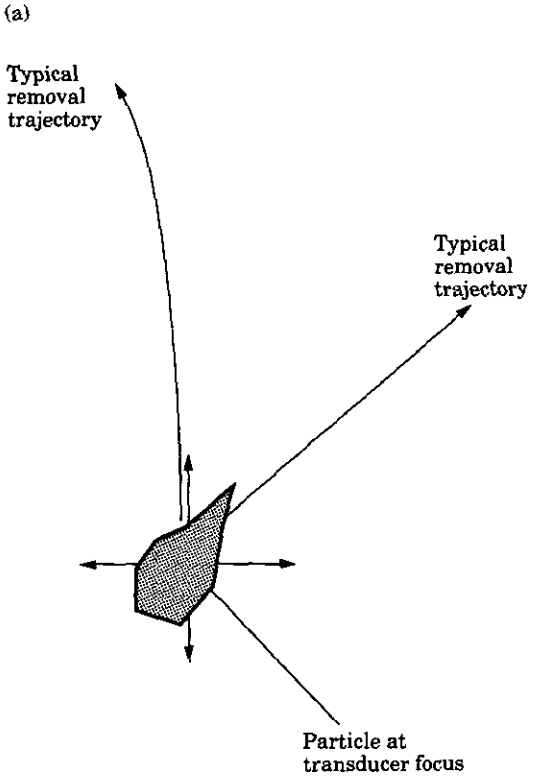

Figure 6. (a) Schematic of experimentally observed trajectories during removal of 2 μm diamond particles under focused ultrasound, viewed perpendicular to the surface. Particles are thought to have only a weak surface-normal velocity component under this mode of removal. (b) A sequence of video images at 1/30 s showing particle removal as the transducer is moved upward with time. Particles are removed at the transducer focus, which is positioned about one-sixth of a screen width to the left of the blurred spot—the right edge of the transducer, which is out of focus.

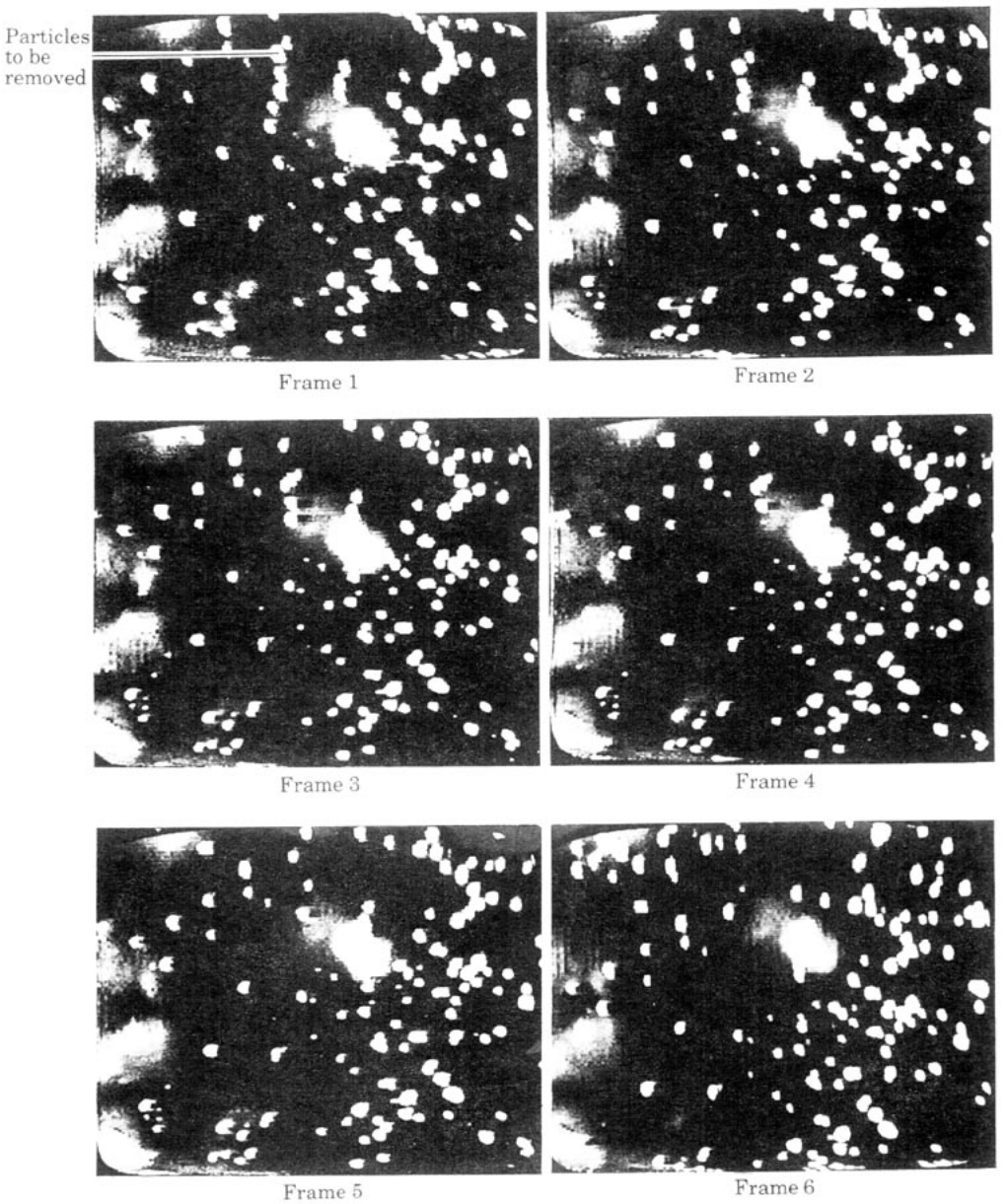

(b)

Figure 6—*continued*

and for the case of particles of around 0·1 μm in diameter, with $h/d \simeq 0{\cdot}01$, this force ratio is of order one.

This *secondary* radiation pressure force is of the correct order to remove submicron particles and so may play a role in mechanisms of particle removal. Its magnitude was compared to the amplitude of the linear oscillatory acoustic force on micron particles by scaling the results of Olson [8], which indicated that r.m.s. oscillatory forces were between 10^2 and 10^3 times greater than the secondary mean force. While it is difficult to speculate

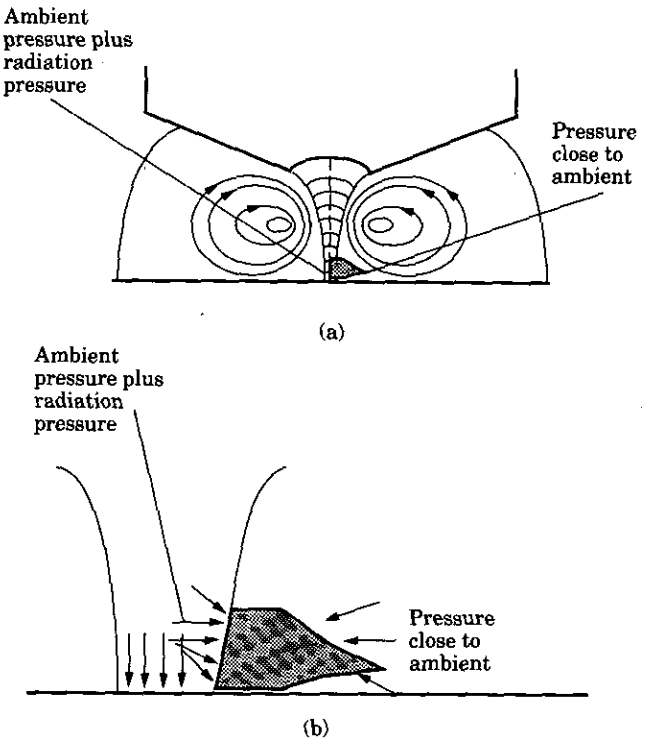

Figure 7. Schematic of the force imbalance on a particle positioned at the edge of a focused acoustic beam, as a result of radiation pressure. The mean force on the particle is approximately normal to the acoustic axis. (a) Total view; (b) detail.

on the precise mechanisms of particle removal, it does appear that secondary non-linear effects of radiation pressure are important. Besides linear oscillation, other contributory effects might include Rayleigh waves travelling along the liquid–solid interface (which might shear particles free), or local thermal dissipation of acoustic energy.

4.3. PARTICLE REMOVAL BY SCANNING

Systematic removal of particles by scanning could be achieved when acoustic excitation was applied at the same amplitude used for particle manipulation, but with excitation over longer continuous periods within the transducer duty cycle. For continuous wave excitation at mean energy densities of $\langle E \rangle \simeq 200\,\mathrm{kN/m^2}$ at the surface, and for higher energy densities applied for progressively shorter periods, all visible particles (1–4 μm diamond, 2–4 μm aluminum and 2–6 μm polystyrene latex) in the path scanned by the transducer path were removed. Their trajectories were in planes almost normal to the acoustic axis, and may be viewed on the companion videotape to reference [24]. The similarities between this mechanism of removal and that observed for manipulation by excitation over shorter duty cycles implied that the former was a more vigorous version of the latter. If secondary acoustic forces were to control particle removal, extensions of this technique to submicron particles would then depend on the ability to design acoustic lenses with fine focusing capabilities and sufficiently high power ratings.

5. CONCLUDING REMARKS

An experimental investigation of particle removal by focused ultrasound has been combined with analytical and computational modelling to explore some features of micron

particle removal. Experimental results indicate that successful removal of particles depends on both acoustic energy density and exposure time, and that the mechanism of removal involves more than just the frequency and amplitude of acoustic excitation. The general agreement of modelled effects with experimental observation implies that secondary forces of radiation pressure may be of importance in mechanisms of particle removal.

Focused ultrasound has also been shown to have attractive features such as ease of control over acoustic power and frequency, fine resolution and predictable acoustic streaming motions. Better models for radiation pressure around particles at surfaces, improved understanding of focused beam acoustics, and a refined understanding of particle removal mechanisms could then lead to more advanced devices. These could be both cleaning tools and remote diagnostics instruments which might estimate the surface-attractive forces acting on individual particles and so qualify the suitability of other cleaning techniques.

ACKNOWLEDGMENTS

The authors gratefully acknowledge the financial support of the IBM Research Division, Thomas J. Watson Research Center, and the assistance of Professor V. Liepa and Mr M. Schuck.

REFERENCES

1. P. M. Morse 1976 *Vibration and Sound.* New York: American Institute of Physics Press.
2. L. V. King 1934 *Proceedings of the Royal Society London* **A147**, 212–240. On the acoustic radiation pressure on spheres.
3. K. Y. Yosioka and Y. Kawasima 1955 *Acoustica* **5**, 167–173. Acoustic radiation pressure on a compressible sphere.
4. T. F. W. Embleton 1954 *Journal of the Acoustical Society of America* **26**, 40. Mean force on a sphere in a spherical sound field, I: theoretical.
5. T. F. W. Embleton 1956 *Canadian Journal of Physics* **34**, 276. On the radiation force on a spherical obstacle in a cylindrical sound field.
6. S. D. Danilov and M. A. Mironov 1984 *Soviet Physics—Acoustics* **30**, 280. Radiation pressure force acting on a small particle in a sound field.
7. S. Temkin and C.-M. Leung 1976 *Journal of Sound and Vibration* **49**, 75–92. On the velocity of a rigid sphere in a sound wave.
8. L. G. Olson 1988 *Journal of Sound and Vibration* **126**, 387–405. Finite element model for ultrasonic cleaning.
9. L. G. Olson 1993 *Journal of Sound and Vibration* **161**, 137–156. A simplified finite element model for ultrasonic cleaning.
10. T. L. Geers and M. Hasheminejad 1991 *Journal of the Acoustical Society of America* **90**, 3238–3247. Linear analysis of an ultrasonic cleaning problem.
11. J. Reed 1989 in *Particles on Surfaces* 2 (K. L. Mittal, editor), 3–18. New York: Plenum Press. The adhesion of small particles to a surface.
12. V. B. Menon, L. D. Michaels, R. P. Donovan and D. S. Ensor 1989 in *Particles on Surfaces* 2 (K. L. Mittal, editor), 297–306. New York: Plenum Press. Ultrasonic and hydrodynamic techniques for particle removal from silicon wafers.
13. D. M. Berg, T. Grimsley, P. Hammond and C. T. Sorenson 1989 in *Particles on Surfaces* 2 (K. L. Mittal, editor), 307–316. New York: Plenum Press. New sonic cleaning technology for particle removal from semiconductor surfaces.
14. G. W. Willard 1953 *Journal of the Acoustical Society of America* **25**, 669–686. Ultrasonically induced cavitation in water: a step-by-step process.
15. I. Kashkoush and A. Busnaina 1991 *Proceedings of the Institute of Environmental Sciences, 37th Annual Meeting, San Diego*, 861–867. Submicron particle removal from surfaces using acoustic streaming.
16. K. L. Mittal (editor) 1988 *Particles on Surfaces* 1. New York: Plenum Press.

17. K. L. MITTAL (editor) 1989 *Particles on Surfaces* 2. New York: Plenum Press.
18. R. T. BEYER 1974 *Nonlinear Acoustics*. Washington, D.C.: Department of the Navy.
19. J. LIGHTHILL 1978 *Journal of Sound and Vibration* **61**, 391–418. Acoustic streaming.
20. M. H. SCHUCK 1990 *M.S. Thesis, The University of Michigan*. Removal of submicron contaminants from silicon wafers using focused acoustic waves.
21. L. D. ROZENBERG 1971 *High-intensity Ultrasonic Fields*. New York: Plenum Press.
22. A. D. GOSMAN, W. M. PUN, A. K. RUNCHAL, D. B. SPALDING and M. WOLFSHTEIN 1969 *Heat and Mass Transfer in Recirculating Flows*. London: Academic Press.
23. K. A. NAUGOL'NYKH, S. I. SOLUYAN and R. V. KHOKHLOV 1963 *Soviet Physics—Acoustics* **9**, 42. Spherical waves of finite amplitude in a viscous thermally conducting medium.
24. G. J. BRERETON and B. A. BRUNO 1992 *International Video Journal of Engineering Research* **2**, 3–16. Manipulation and removal of micron particles by focused acoustic waves.
25. H. G. B. CASIMIR and D. POLDER 1948 *Physical Review* **73**, 360–372. The influence of retardation on the London – van der Waals forces.
26. D. LEIGHTON and A. ACRIVOS 1985 *Journal of Applied Mathematics and Physics (ZAMP)* **36**, 174–178. Lift force on a small sphere in the presence of a wall.
27. B.-T. CHU and R. E. APFEL 1982 *Journal of the Acoustical Society of America* **72**, 1673–1687. Acoustic radiation pressure produced by a beam of sound.